AR-009-940

DSTO-RR-0091

DSTO

Geometric and Radiometric Image Warping due to Displacement of Wide Field Optical Systems

Robert S. Caprari

DEPARTMENT OF DEFENCE

DEFENCE SCIENCE AND TECHNOLOGY ORGANISATION

Geometric and Radiometric Image Warping due to Displacement of Wide Field Optical Systems

Robert S. Caprari

Land, Space and Optoelectronics Division
Electronics and Surveillance Research Laboratory

DSTO-RR-0091

ABSTRACT

This report investigates a problem that arises in the precise registration of images viewed from a moving wide field imaging sensor, such as an airborne missile threat warner. It analyses the geometry and radiometry of image formation by idealised, but otherwise arbitrary, imaging optics, thereby determining the image plane irradiance distribution. The analysis extends to determining the transformation of the irradiance (i.e. image warping) due to arbitrary displacement of the optical system; such image warping being separable into geometric (i.e. image point shift) and radiometric (i.e. intensity scaling) components. Numerical simulations demonstrate the severity of the radiometric warping for wide field images—an especially important result, since radiometric warping is conventionally neglected in image registration. Exact solutions for the warping due to pure rotation of an idealised imager are presented. These are completely independent of the scene. An examination of the inclusion of imager translation shows that the warping becomes formally dependent on the scene topography, and emission/scattering directionality. Simulations of the use of block matching to achieve approximate registration are presented.

DEPARTMENT OF DEFENCE

DEFENCE SCIENCE AND TECHNOLOGY ORGANISATION

Published by

DSTO Electronics and Surveillance Research Laboratory
PO Box 1500
Salisbury, South Australia, Australia 5108

Telephone: (08) 8259 5555
Facsimile: (08) 8259 6567

AR No. AR-009-940

December 1996

APPROVED FOR PUBLIC RELEASE

Geometric and Radiometric Image Warping due to Displacement of Wide Field Optical Systems

EXECUTIVE SUMMARY

For quite some time, Land, Space and Optoelectronics Division has maintained an ongoing research programme on electro-optic missile threat warners. This has involved exploration and development of possible new forms of threat warner, as well as assessment of existing systems. As a further contribution to this research effort, this report addresses an important problem that arises in threat warning systems based on the detection of changes (due to motion of an approaching missile against the background) in wide field images acquired by passive sensors. The problem of concern is that of the need for pre-warping of image geometries and intensities, prior to image subtraction for the purposes of accentuating real changes in the scene.

The following airborne threat warning system is considered. An aircraft is fitted with a downward looking, very wide field imager. Images consist of the landscape beneath the aircraft, and possibly an approaching missile. Consecutive images are subtracted from one another to eliminate the stationary background clutter, but leave a signature at the location of the fast moving missile.

A fundamental problem with this missile detection scheme for an imager mounted directly on the airframe, is that the imager wobbles as the aircraft rolls, pitches and yaws. Consecutive images will therefore correspond to different orientations of the imager, so that direct subtraction of images will not completely eliminate the background clutter. It is necessary to transform images to a common imager reference frame (i.e. the images must be registered), before they are subtracted.

Wide field imaging has two peculiarities that are either nonexistent or not apparent in the narrow field perfect imaging case that is usually assumed. The first is that wide field imaging optics are deliberately designed to be geometrically distorting, to keep the image size within the limits of a focal plane detector. Narrow field optics generally have negligible geometric distortion. The second peculiarity is that the radiometric (i.e. intensity) distortion that is generally present in any imaging system, only becomes significant at large field angles, hence it is only significant in wide field images.

This report analyses idealised wide field imaging optics to describe how object position and radiance are transformed into the image plane, and how this transformation varies with arbitrary displacement of the optical system. It is this variation of the transformation with optical system displacement that gives rise to the need for registration of images by a warping operation. Furthermore, simulations demonstrate that a radiometric transformation (pixel intensity transformation) is required in addition to a geometric transformation (pixel position transformation) in order to achieve registration.

For pure rotation of the imaging sensor, the report shows that the exact solution for the geometric and radiometric warping needed to register two images depends on only the sensor motion and optical characteristics, but not on any scene properties. From an

imaging perspective, the condition of pure rotation is a close approximation to the actual motion of a slow or high flying aircraft, or a particularly unsteady one. If the sensor also undergoes translation, the report reveals how the exact solution also depends on the scene topography and its directionality of emission or scattering.

Simulations of block matching approximations to the exact registration problem are presented. Block matching entails partitioning one image into an array of subimages, and registering each subimage with the other image by simple translation only. At least for the present example, it seems that block matching can accommodate geometric warping quite well, but less so for radiometric warping. A meaningful measure of the precision achieved by any approximate registration algorithm depends on the scene as well as the optical system and its displacement. An average precision value will require testing of the approximate algorithm on a large ensemble of scenes, or alternatively, a statistical analysis based on good stochastic models for the radiance and surface variation of the scene.

Authors

Robert S. Caprari
Land, Space and Optoelectronics Division

Robert Caprari did his undergraduate study at Adelaide University, obtaining the degrees of Bachelor of Engineering (Honours) and Bachelor of Science, the former majoring in electrical and electronic engineering, and the latter majoring in physics. He then joined Optoelectronics Division of DSTO as a Professional Officer 1, and did research in image processing and imaging system characterisation, before joining Electronic Warfare Division as a Professional Officer 2, and doing research in mathematical and acoustooptic techniques of radio frequency signal detection and identification. On obtaining DSTO sponsorship as a Cadet Research Scientist, he conducted research in experimental and theoretical condensed matter and electron scattering physics at Flinders University, obtaining the degree of Doctor of Philosophy. Subsequently, he joined Land, Space and Optoelectronics Division in his current position as a Research Scientist, undertaking research into the physics of imaging, and statistical signal theory and computation.

THIS PAGE IS INTENTIONALLY BLANK

Contents

THIS PAGE IS INTENTIONALLY BLANK

1 Introduction

The research reported here was motivated by a problem that arose in a previous proposal for a passive, airborne missile approach warning system (Caprari [1]). The concept underlying this proposal is to have an imaging sensor view the scene below the aircraft. Consecutive images would be carefully registered, both geometrically and radiometrically (i.e. in intensity), so that subtraction of the images would in principle leave a residual only where a fast moving missile is located. Image registration is the process of transforming two images of ostensibly the same scene, so that a given object point appears at the same image point and with the same intensity in both images. It is envisaged that the imaging system required for passive threat warning would have simultaneous coverage of almost all of the hemisphere below the aircraft, that is, a field of view approaching 180°. The imaging system is assumed to be mounted directly on the airframe, without a gyroscopically stabilised mount. Consequently, the optical axis of the imaging system rotates as the aircraft rolls, pitches and yaws, with the result that consecutive images are warped relative to each other.

The fundamental problem in this type of passive missile detection scheme is one of registration of consecutive images obtained by a system that both translates and rotates in the time period between the acquisition of the two images. And the precision of registration demanded by this missilie detection scheme is extreme. In fact, the simulations contained in the report on this scheme by Caprari [1] assume perfect image registration, and yet the missile detection capability of this scheme is still only assessed as being marginal. Furthermore, the missile detection capability declines with declining precision of image registration.

This report presents the exact solution to this problem, for an idealised wide field imager with known motion. The exact geometric transformation between images is shown to be of such complexity that it can not be represented by a global image translation, which is an often used approximation. Furthermore, the exact radiometric transformation, which is often neglected in image registration, will be seen to be significant for the wide field images of interest in passive airborne missile threat warning.

As an approximation to the exact image transformation, this report examines the partitioning of one of the images into subimages, and independently registering each subimage with the other image, using only translation and intensity scaling. Such an approach to image registration would be appropriate if the parameters specifying the exact transformation, being the Euler angles of imaging system rotation in this case, were not known with sufficient precision. Estimation of the translation and intensity scaling parameters is done on the basis of minimising the difference between the transformed subimage and the other image, using an iterative procedure. The best estimate would in principle depend on the content of the image, whereas the exact transformation does not. Although a global image translation and intensity scaling is a poor approximation to the exact transformation, it will be seen that the same type of approximation independently applied to sufficiently small subimages can be a reasonably good approximation. The importance of this result is that it implies that even if imaging system orientation information is not available in a proposed missile detection system, the likelihood is that sufficiently precise image

registration can still be undertaken by a conceptually simple approximation procedure.

Fundamentally, this report seeks to quantify how a changing optical system disposition relative to the scene influences the way that scene is imaged, with particular emphasis on wide field imaging. Such information is of critical importance for the effective and precise geometric and radiometric registration of sequences of images. In addition to the application that has motivated this report, this operation is important in applications such as: temporal noise suppression by image summation (temporally white noise is reduced by a factor of $\sqrt{N}$ by summing N images); change detection by image subtraction (the consequences of inaccurate image registration on the reliability of change detection have been investigated by Townshend *et al* [2]); and computer based image stabilisation for presentation on a display as a substitute for mechanical stabilisation of the imaging platform (see Bonshtedt *et al* [3] and references therein).

The contents of this report are summarised as follows. Section 2 introduces the notion of imaging characteristic, related to the distortion aberration of image formation, and specifies a feasible imaging charcteristic for a wide field imaging system. Section 3 discusses the kinematics of rotation, and the Euler angles parametrisation of rotation. Section 4 presents the formal expression for allowable image transformations, from which it is evident that any transformation naturally separates into a geometric and radiometric (intensity) component. Section 5 analyses the geometric warping resulting from camera rotation, and includes simulation results. Section 6 analyses the radiometric warping resulting from camera rotation, and includes simulation results. Section 7 indicates how the preceding analyses are modified to include camera translation also, and discusses the ensuing complications for both warping components.

This report is an enhanced version of an article published by the author in the open literature (Caprari [4]).

2 Imaging characteristic

Consider an axially symmetric optical system. The image formation of the optical system is assumed to be stigmatic for all object points (depth of field extends over the complete radial distance variation of the object), hence the only permissible aberrations are curvature of field and distortion. Curvature of field is assumed to be absent, thus leaving distortion as the only aberration. The imaging geometry of an arbitrary optical system of this type is illustrated in Figure 1.

Image distortion is quantified by expressing the relation between θ, the polar angle of the object point measured with respect to the optical axis, and ρ, the radial distance of the image point from the centre of the image plane:

$$\rho = F(\theta) \ , \ \text{for } \theta > 0 \ . \tag{1}$$

The origin of the vertex measured by θ is the (real or virtual) intersection of the object space chief ray with the optical axis; for an aperture stop centred on the optical axis, this is just the centre of the entrance pupil. One will appreciate from the analysis of radiometric

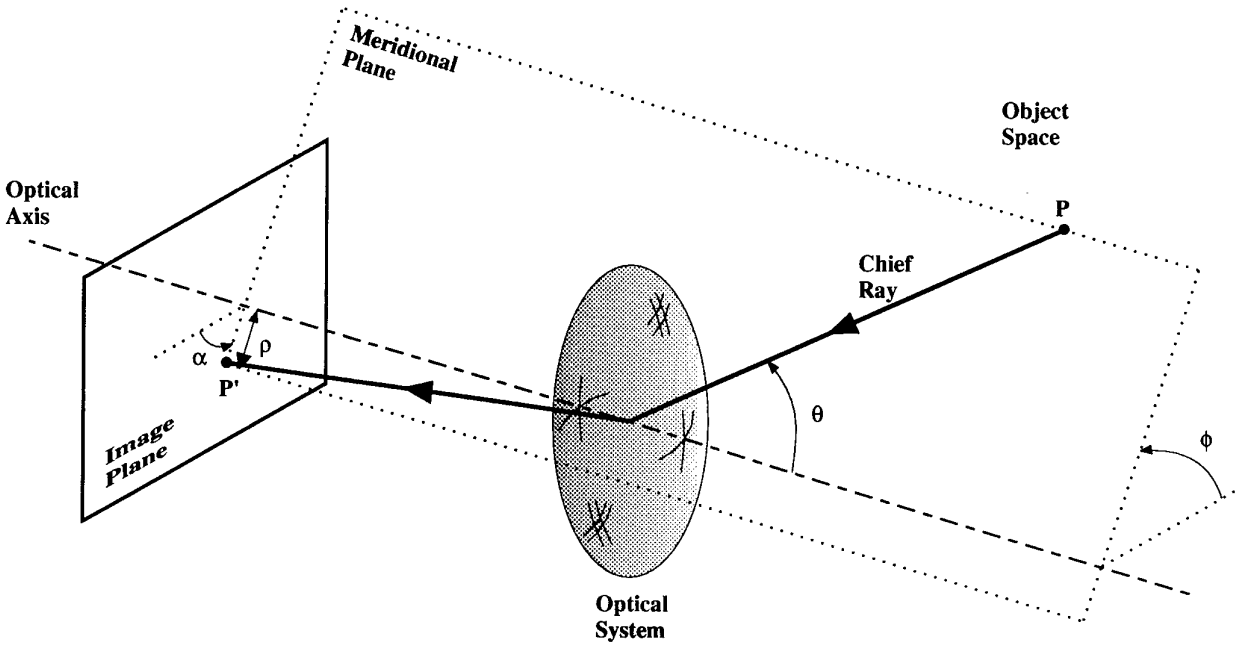

Figure 1: The geometry of image formation by an arbitrary axially symmetric optical system whose only aberration is distortion. For a multi-component optical system, the vertex about which θ is measured is actually the centre of the entrance pupil.

warping in Section 6 why the origin of object space is chosen to be the centre of the entrance pupil, rather than one of the cardinal points of the optical system. Conjugate object and image points are located in the same meridional plane, which also contains the optical axis. One may arrange the object space and image plane coordinate systems so that the object point azimuthal angle ϕ equals the image point azimuthal angle α, that is,

$$\alpha = \phi \ . \tag{2}$$

One may introduce the term *imaging characteristic* of the optical system (not to be confused with a Hamiltonian characteristic function) to denote the function $F(\theta)$. $F(\theta)$ certainly would be monotonically increasing from $F(0)=0$ for any sensible imaging system.

The perfect imaging approximation, in which there is no image distortion, corresponds to the imaging characteristic,

$$F_{\text{perfect}}(\theta) = f \tan\theta \qquad \text{(perfect imaging)} \ , \tag{3}$$

where, for an object effectively at infinity, f is the focal length of the optical system. This imaging characteristic is both atypical and undesirable for very wide angular field of view optical systems ($2\theta_{\text{max}} \gtrsim 100°$). It is particularly undesirable in circumstances where the optical system has an area photodetector without mechanical scanning, where there are

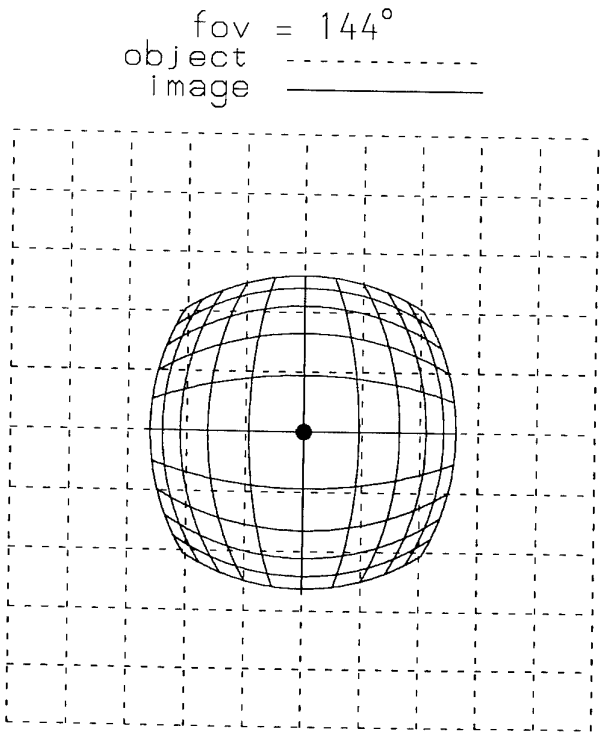

Figure 2: Visual representation of the imaging characteristic $F(\theta)=f\theta$, where f is chosen to give unity central magnification, and the four vertices of the object grid correspond to the polar angle $\theta = 72°$. The small filled circle indicates the position of the optical axis (which is normal to both object and image), that is, $\theta=0$. The observable barrel distortion deviates from Seidel distortion.

severe constraints on the maximum size of the photodetector (eg. monolithic focal plane array). In such a situation there is an inherent incompatibility between the asymptotically infinite image area arising from (3), and the finite and small area photosensitive region in the image plane.

An imaging characteristic that alleviates this problem by producing smaller images, and one that is more representative of actual wide field of view optical systems, is,

$$F(\theta) = f\theta \qquad \text{(actual imaging)} \ , \tag{4}$$

where the object point polar angle θ is expressed in radians. Examples of imaging systems that conform to imaging characteristic (4) include some *fish eye* lenses (Miyamoto [5], Kingslake [6, Secs. 6.II.A and 15.V.C]), the *Zeiss Pleon* lens (Gardner and Washer [7]), and several contemporary designs (eg. Kawamura [8], Hayashida [9]). The image distortion associated with imaging characteristic (4) is illustrated in Figure 2, for the special case of unity central magnification and angular field of view $2\theta_{\max} = 144°$. Inspection of Figure 2 immediately reveals that imaging characteristic (4) exhibits barrel, or positive, distortion.

The geometric distortion $\Delta\rho(\theta)$ of an arbitrary imaging characteristic is its deviation from the perfect imaging characteristic, that is,

$$\Delta\rho(\theta) \equiv F(\theta) - F_{\text{perfect}}(\theta) \ . \tag{5}$$

For the presently assumed imaging characteristic, one has from (3) and (4),

$$\begin{aligned} \Delta\rho(\theta) &= f\theta - f\tan\theta \ , \\ &= -\tfrac{1}{3}f\theta^3 - \tfrac{2}{15}f\theta^5 + \mathcal{O}(\theta^7) \qquad (|\theta| < \frac{\pi}{2}) \ , \\ &= -\tfrac{1}{3}f\tan^3\theta + \tfrac{1}{5}f\theta^5 + \mathcal{O}(\theta^7) \qquad (|\theta| < \frac{\pi}{2}) \ . \end{aligned} \tag{6}$$

Since primary, or Seidel, distortion has the form (see any geometrical optics textbook),

$$\Delta_{\text{Seidel}}\rho(\theta) \propto \tan^3\theta \qquad \text{(Seidel distortion)} \ , \tag{7}$$

one observes from (6) that the actual distortion associated with imaging characteristic (4) deviates from Seidel distortion.

Given an arbitrary imaging optical system, it is a relatively simple matter to measure experimentally its imaging characteristic $F(\theta)$ (see Shah and Aggarwal [10], and references therein).

3 Optical system rotation

Consider the aircraft initially pointing along the x-axis, the right wing approximately pointing along the y-axis, and the downward directed imager optical axis pointing along the z-axis (Figure 3). Rotation of the aircraft and imaging system is specified by the three independent *Euler angles* ϕ, θ and ψ (Goldstein [11, Sec. 4-4 and App. B]), defined according to the following convention:

1. The first rotation is by angle ϕ around the original z-axis (*yaw* or *heading*).

2. The second rotation is by angle θ around the intermediate y-axis (*pitch* or *attitude*).

3. The third rotation is by angle ψ around the final x-axis (*roll* or *bank*).

The orientation of the aircraft and imaging system changes from being aligned with axes (x, y, z) to being aligned with axes (x', y', z'). Such a rotation is defined by specific values of Euler angles ϕ, θ and ψ. The linear transformation between the cartesian coordinates of an invariant object space point in the initial and final reference frames is expressed by,

$$\mathbf{r}' \ = \ \mathbf{T}(\phi, \theta, \psi)\mathbf{r} \ , \tag{8}$$

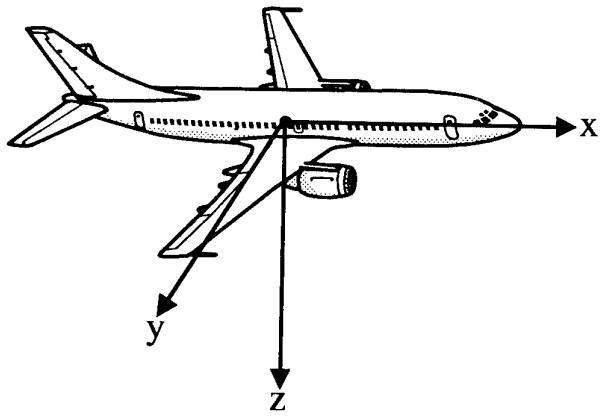

Figure 3: Cartesian coordinates defined with respect to an aeroplane carrying an imaging system with optical axis along the z-axis. The origin coincides with the centre of the entrance pupil of the optical system.

where $\mathbf{r}$ implicitly represents the column vector of cartesian coordinates, and the *rotation matrix* $\mathbf{T}$ is,

$$\mathbf{T}(\phi,\theta,\psi) = \begin{bmatrix} \cos\phi\cos\theta & \sin\phi\cos\theta & -\sin\theta \\ \left.\begin{matrix}\cos\phi\sin\theta\sin\psi- \\ \sin\phi\cos\psi\end{matrix}\right) & \left.\begin{matrix}\sin\phi\sin\theta\sin\psi+ \\ \cos\phi\cos\psi\end{matrix}\right) & \cos\theta\sin\psi \\ \left.\begin{matrix}\cos\phi\sin\theta\cos\psi+ \\ \sin\phi\sin\psi\end{matrix}\right) & \left.\begin{matrix}\sin\phi\sin\theta\cos\psi- \\ \cos\phi\sin\psi\end{matrix}\right) & \cos\theta\cos\psi \end{bmatrix} . \quad (9)$$

The linear transformation represented by $\mathbf{T}$ is a proper orthogonal transformation, that is,

$$\mathbf{T}^{-1} = \mathbf{T}^{T} , \quad (10)$$

$$\det \mathbf{T} = 1 . \quad (11)$$

Conversely, given an arbitrary orthogonal transformation $\mathbf{T}$ with matrix elements t_{ij}, $i,j = 1,2,3$, one may deduce three Euler angles that completely parametrise $\mathbf{T}$ as follows,

$$\begin{array}{lcll} \phi & = & \arctan(t_{12}/t_{11}) & \text{(quadrant determined by signs of } t_{12} \text{ and } t_{11}) \ , \\ \theta & = & -\arcsin(t_{13}) & \theta \in [-\pi/2, \pi/2] \ , \\ \psi & = & \arctan(t_{23}/t_{33}) & \text{(quadrant determined by signs of } t_{23} \text{ and } t_{33}) \ . \end{array} \quad (12)$$

The very same orthogonal transformation is equally well parametrised by another set of Euler angles for which $\theta \in [\pi/2, 3\pi/2]$.

To the extent that the landscape is planar on the macroscopic scale, even though on the microscopic scale the topography may be quite rough, it is possible to define an object plane of best fit. A standard object space frame of reference $O(x,y,z)$ is arbitrarily

defined to have its origin at the centre of the entrance pupil, with its z-axis normal to, and pointing towards, the object plane. It follows that the xy-plane is parallel to the object plane. Frame O is denoted the *cardinal* frame of reference.

Reference frame $O_0(x_0, y_0, z_0)$ is aligned along the initial optical system orientation, in particular, the z_0-axis is the initial optical axis. The orientation of frame O_0 with respect to frame O is specified by the Euler angle values ϕ_0, θ_0 and ψ_0. From (8), the coordinate transformation from O to O_0 is,

$$\mathbf{r}_0 = \mathbf{T}_0\mathbf{r} \ , \tag{13}$$

where,

$$\mathbf{T}_0 \equiv \mathbf{T}(\phi_0, \theta_0, \psi_0) \ . \tag{14}$$

Similarly, reference frame $O_1(x_1, y_1, z_1)$ is aligned along the final optical system orientation, in particular, the z_1-axis is the final optical axis. The orientation of frame O_1 with respect to frame O is specified by the Euler angle values ϕ_1, θ_1 and ψ_1. From (8), the coordinate transformation from O to O_1 is,

$$\mathbf{r}_1 = \mathbf{T}_1\mathbf{r} \ , \tag{15}$$

where,

$$\mathbf{T}_1 \equiv \mathbf{T}(\phi_1, \theta_1, \psi_1) \ . \tag{16}$$

Transforming in turn from frame O_0 to frame O and then from frame O to frame O_1, one obtains the transformation of object space coordinates from O_0 to O_1, that is, from the initial optical system orientation to the final optical system orientation:

$$\mathbf{r}_1 = \mathbf{T}_{01}\mathbf{r}_0 \ , \tag{17}$$

where,

$$\mathbf{T}_{01} = \mathbf{T}_1\mathbf{T}_0^T \ . \tag{18}$$

Orthogonality condition (10) has been invoked in obtaining (18).

$\mathbf{T}_{01}$ is also a proper orthogonal transformation; that is, it represents a single rotation. In particular, $\mathbf{T}_{01}$ is the effective rotation that can displace the optical system from its initial orientation to its final orientation (regardless of the actual trajectory of the optical system in accomplishing its displacement). Consequently, $\mathbf{T}_{01}$ must be completely parametrised by the effective Euler angles ϕ_{01}, θ_{01} and ψ_{01}, determined from its matrix elements according to (12).

Although transformation $\mathbf{T}_{01}$ may be effected without recourse to subsidiary transformations $\mathbf{T}_0$ and $\mathbf{T}_1$, the utility of introducing $\mathbf{T}_0$ and $\mathbf{T}_1$ will become evident in Section 7. As an alternative to the rotation matrix $\mathbf{T}_{01}$, the direct transformation of polar coordinates ensuing from a rotation of the reference frame may be expressed by the equations in Appendix A.

4 General image warping

An optical system whose only aberration is distortion will project stigmatic images of a scene that are distorted compared with any projective transformation of the scene. If the optical system is moving, there is also a temporal variation of the image of an essentially constant scene. This image-to-image spatial and amplitude variation constitutes the image warping that is of particular interest in this exposition. The distinction between distortion and warping is that, whereas the former is present in a single image due to lens aberration, the latter is fundamentally a property of a sequence of images. Distinguishing between distortion and warping in this manner facilitates discussion by eliminating ambiguity between these two concepts.

The warping between images projected 'before' and 'after' an optical system displacement can be expressed algebraically as follows. Define,

$$\begin{array}{rcl} (x_0, y_0) & \equiv & \text{points on the initial image plane} \ , \\ s_0(x_0, y_0) & \equiv & \text{initial image intensity distribution} \ , \\ (x_1, y_1) & \equiv & \text{points on the final image plane} \ , \\ s_1(x_1, y_1) & \equiv & \text{final image intensity distribution} \ . \end{array} \tag{19}$$

One is cautioned that the term 'image intensity' denotes the image function value (ie. amplitude, grey level or brightness), and is not in accordance with the strict definition of intensity adopted in radiometry; in fact, image intensity actually is the irradiance of radiometry, as acknowledged in (45). The *geometric* transformation from the initial image plane to the final image plane has the general form,

$$\begin{array}{rcl} x_1 & = & X_{01}(x_0, y_0) \ , \\ y_1 & = & Y_{01}(x_0, y_0) \ , \end{array} \tag{20}$$

which may be regarded as a vector field in the x_0y_0-plane. The *radiometric*, or intensity, transformation from the initial image plane to the final image plane has the general form,

$$s_1(x_1, y_1) = R(x_0, y_0, x_1, y_1) s_0(x_0, y_0) \ , \tag{21}$$

which may be regarded as a scalar field in the x_0y_0-plane.

Note that R in (21) is implicitly a function of only (x_0, y_0), since (x_1, y_1) is completely determined by (x_0, y_0) according to (20); therefore R often will be simply expressed as $R(x_0, y_0)$. Note also that (21) implies that a general radiometric transformation is completely determined by the positions in the image planes, regardless of illumination conditions, or reflection and emission directional characteristics of the object surface. The extent to which this is so will be investigated in Sections 6 and 7. The intensity linearity of image formation (assuming the use of only linear optical elements) is reflected in the form of (21), by the fact that R does not depend on s_0, so that final image intensities are simply proportional to initial image intensities. Substitution of (20) into (21) entirely specifies the most general physically allowable point transformation that quantifies the image warping between two images of the same scene.

Of particular interest in this report is the special case of the two images being those projected by an optical system before and after a rotation. In this circumstance, the image

warping is uniquely specified; exactly how will be revealed in Section 5 for the geometric component of the warping, and Section 6 for the radiometric component of the warping. Modifications and complications to the pure rotation case that arise on inclusion of a simultaneous translation will be detailed in Section 7.

5 Geometric warping due to optical system rotation

Geometric warping in sequences of undistorted images is frequently studied by imaging science researchers, albeit in a diversity of contexts. Merchant [12] addresses geometric warping of undistorted images due to arbitrary camera displacement, in a context similar to the research that has motivated this report. Geometric warping in pairs of undistorted images is also the essence of the *relative orientation* problem of photogrammetry (Horn [13, 14]), which is actually the inverse problem to the one of interest here. Solving the relative orientation problem entails deducing the camera displacement from specified geometric warping between two undistorted images. In the present report one considers the problem of deducing the geometric warping resulting from specified camera displacement; and doing so for arbitrarily distorted images, that is, for an arbitrary imaging characteristic $F(\theta)$.

Specification of the geometric warping (20) is communicated with greatest clarity by the following algorithm, rather than a self-contained, but complicated, equation. Nevertheless, the closed form solution for geometric warping is stated in Appendix A without derivation.

Step 1. The initial image plane point (x_0, y_0) is expressed in plane polar coordinates (ρ_0, α_0),

$$\begin{aligned} \rho_0 &= (x_0^2 + y_0^2)^{1/2} \ , \\ \alpha_0 &= \arctan(y_0/x_0) \qquad \text{(quadrant determined by signs of } y_0 \text{ and } x_0) \ . \end{aligned} \tag{22}$$

Step 2. Identify the point in object space that is conjugate to image point (x_0, y_0). This object space point has spherical polar coordinates (r_0, θ_0, ϕ_0) with respect to reference frame O_0, which has its z-axis aligned along the initial optical axis, and its origin at the centre of the initial entrance pupil. The axial symmetry property of the optical system unambiguously determines the azimuthal angle ϕ_0, and the particular imaging characteristic uniquely determines the polar angle θ_0. However, the radial distance r_0 is determined by the topography of the scene, which will not be specified for the present. One obtains,

$$\begin{aligned} r_0 &= r \ , \\ \theta_0 &= F^{-1}(\rho_0) \ , \\ \phi_0 &= \alpha_0 \ . \end{aligned} \tag{23}$$

r is the unspecified distance between the optical system and the object point. F^{-1} is the inverse function of F, that is, the inverse imaging characteristic, and is unambiguously

defined since F is a one-to-one function. For the 'fish eye' imaging characteristic (4), one obtains,

$$F^{-1}(\rho) = \frac{1}{f}\rho \qquad \text{(fish eye lens)} \ . \tag{24}$$

The cartesian coordinates of the object point (x'_0, y'_0, z'_0) in frame O_0 are,

$$\begin{aligned} x'_0 &= r_0 \sin\theta_0 \cos\phi_0 \ , \\ y'_0 &= r_0 \sin\theta_0 \sin\phi_0 \ , \\ z'_0 &= r_0 \cos\theta_0 \ . \end{aligned} \tag{25}$$

For present purposes, primed cartesian coordinates represent object space points, and unprimed cartesian coordinates the conjugate image plane points.

Step 3. The cartesian coordinates of the invariant object space point in the rotated frame of reference O_1, which has its z-axis aligned along the final optical axis, and its origin at the centre of the final entrance pupil (which coincides with the origin of O_0 for pure rotation), are given by linear transformation (18),

$$\begin{bmatrix} x'_1 \\ y'_1 \\ z'_1 \end{bmatrix} = \mathbf{T}_{01} \begin{bmatrix} x'_0 \\ y'_0 \\ z'_0 \end{bmatrix} \ . \tag{26}$$

Converting cartesian coordinates (x'_1, y'_1, z'_1) to spherical polar coordinates (r_1, θ_1, ϕ_1) with respect to reference frame O_1, one obtains,

$$\begin{aligned} r_1 &= (x'^2_1 + y'^2_1 + z'^2_1)^{1/2} \ , \\ \theta_1 &= \arctan[(x'^2_1 + y'^2_1)^{1/2}/z'_1] \qquad \theta_1 \in [0, \pi] \ , \\ \phi_1 &= \arctan(y'_1/x'_1) \qquad \text{(quadrant determined by signs of } y'_1 \text{ and } x'_1) \ . \end{aligned} \tag{27}$$

Note that the orthogonality property of transformation $\mathbf{T}_{01}$, together with (23), ensures that for pure rotation,

$$r_1 = r_0 = r \qquad \text{(pure rotation)} \ . \tag{28}$$

Examination of (23), (25), (26) and (27) in sequence, reveals that neither θ_1 nor ϕ_1 depend on r. This condition is a result of the absence of camera translation; camera displacement is being restricted to pure rotation for the present. For a slow moving or high altitude camera platform (ie. aircraft), or a particularly unsteady one, the contribution of rotation to image warping dominates that of translation; so one is considering a realistic scenario in the present exposition.

Step 4. Identify the final image plane point, with plane polar coordinates (ρ_1, α_1), that is conjugate to the invariant object space point. One directly obtains from (1) and (2),

$$\begin{aligned} \rho_1 &= F(\theta_1) \ , \\ \alpha_1 &= \phi_1 \ . \end{aligned} \tag{29}$$

In particular, the fish eye imaging characteristic (4) is,

$$F(\theta) = f\theta \qquad \text{(fish eye lens)} \ . \tag{30}$$

The final image plane point cartesian coordinates (x_1, y_1) are,

$$\begin{aligned} x_1 &= \rho_1 \cos\alpha_1 \ , \\ y_1 &= \rho_1 \sin\alpha_1 \ . \end{aligned} \tag{31}$$

Since it has already been established that neither θ_1 nor ϕ_1 depend on r, it follows from (29) that the final image plane point does not depend on r either. In summary, for the case of camera displacement being pure rotation, the geometric warping from the initial to final image plane is completely independent of the scene topography.

Steps 1 to 4 constitute the algorithm for evaluating the geometric image warping (20) resulting from pure rotation of the optical system, for specified image distortion $F(\theta)$ and arbitrary object surface topography. For presentation purposes, it is preferable to consider the geometric warping as being the displacement between the image points that are conjugate to the same object point for the initial and final camera orientation, that is,

$$\begin{aligned} g'_x &\equiv x_1 - x_0 \ , \\ g'_y &\equiv y_1 - y_0 \ . \end{aligned} \tag{32}$$

Since (x_1, y_1) is a function of (x_0, y_0), the geometric warping is a vector field in the initial image plane, expressed as $(g'_x(x_0, y_0), g'_y(x_0, y_0))$.

It is best to exclude global image translation from geometric warping; since pure image translation does not conform to one's common notion of warping (ie. there is no difference in the appearance of the images), and also because evaluation of the translation is a simple and well understood 'standard' problem, from the perspectives of analysis, algorithms and hardware implementation (the solution being based upon the cross correlation operation). One achieves this by subtracting the arbitrary global image translation (q_x, q_y) from the geometric warping, and optimising parameters q_x and q_y according to the least squares criterion:

$$\underset{q_x, q_y}{\text{minimum}} \iint\limits_{\substack{\text{complete} \\ \text{image}}} \| (g'_x(x_0, y_0), g'_y(x_0, y_0)) - (q_x, q_y) \|^2 \, \mathrm{d}x_0 \, \mathrm{d}y_0 \ . \tag{33}$$

The solution of (33) is the image translation that best approximates the actual geometric warping in the least squares sense:

$$\begin{aligned} \widehat{q}_x &= \frac{1}{\text{Area}} \iint\limits_{\substack{\text{complete} \\ \text{image}}} g'_x(x_0, y_0) \, \mathrm{d}x_0 \, \mathrm{d}y_0 \ , \\ \widehat{q}_y &= \frac{1}{\text{Area}} \iint\limits_{\substack{\text{complete} \\ \text{image}}} g'_y(x_0, y_0) \, \mathrm{d}x_0 \, \mathrm{d}y_0 \ . \end{aligned} \tag{34}$$

The interpretation of (34) is that the optimum global image translation is just the spatial average of the geometric warping vector field; which is an intuitive result.

One defines the most appropriate geometric warping vector field (g_x, g_y) by,

$$\begin{aligned} g_x &\equiv x_1 - x_0 - \widehat{q}_x \ , \\ g_y &\equiv y_1 - y_0 - \widehat{q}_y \ . \end{aligned} \tag{35}$$

The geometric warping represented by (35) is not quite the intrinsic geometric warping, representing only the non-shape-preserving component of the geometric transformation, since (35) still includes global image rotation. One may quantify the severity of the geometric warping by its root mean square value,

$$g_{\text{RMS}} = \left(\frac{1}{\text{Area}} \iint\limits_{\substack{\text{complete} \\ \text{image}}} \|(g_x(x_0, y_0), g_y(x_0, y_0))\|^2 \, \mathrm{d}x_0 \, \mathrm{d}y_0 \right)^{1/2} . \tag{36}$$

An actual example of the geometric warping vector field (g_x, g_y) is illustrated in Figure 4. In this example, the optical system has the fish eye imaging characteristic (4), as illustrated in Figure 2. The angular field of view is $2\theta_{\text{max}} = 144°$, where θ_{max} is the field angle conjugate to any of the vertices of the square image. Parameter f in (4) is chosen so that the image vertices have cartesian coordinates $(\pm 1, \pm 1)$. The optical system angular displacement is parametrised by the Euler angle values $\phi_{01} = 4°$, $\theta_{01} = -5°$ and $\psi_{01} = -7°$, as discussed in Section 3. Since this example corresponds to pure camera rotation, the geometric warping vector field is completely independent of the actual scene and its topography. A global image translation of $(\widehat{q}_x, \widehat{q}_y) = (0.09, -0.12)$ units has been excluded from the geometric warping vector field. The root mean square geometric warping is $g_{\text{RMS}} = 0.057$ units.

Inspection of Figure 4 reveals that the geometric warping vector field has a clockwise circulation that may be partially removed by excluding an appropriate global image rotation. However, it is evident that one can not account for the totality of geometric warping by only proper shape-preserving image tranformations (ie. translation and rotation, but not reflection). There is an intrinsic geometric warping present that represents change of shape. Inspection of Figure 4 also suggests that, generally, geometric warping increases with increasing field angle θ. This conclusion follows from the observation that geometric warping generally tends to increase with distance from the optical axis (ie. image centre).

A common approach to the registration of two mutually warped images of the same scene, is to isolate a small region in one image, and maximise the cross correlation of the second image with this small region (see, for example, Pritt [15]). This technique is termed block matching in image registration. The justification for this approach is that the geometric warping in a small region is very approximately a local translation, since other terms in the Taylor series expansion are not too large. Different regions will have different local translation vectors. The present analysis allows one to quantify the benefits of this approach.

Figure 5 illustrates the geometric warping vector field for identical parameter values to those of Figure 4. The difference is that in Figure 5 the image is partitioned into 4×4 subimages of equal size, and the geometric warping in each subimage is 'corrected' for its own subimage translation. Different subimages have different optimal translations. The geometric warping fields of Figures 4 and 5 are otherwise identical.

Comparison of Figures 4 and 5 certainly does verify that operating on small image segments reduces the severity of geometric warping. A quantitative indication of this is

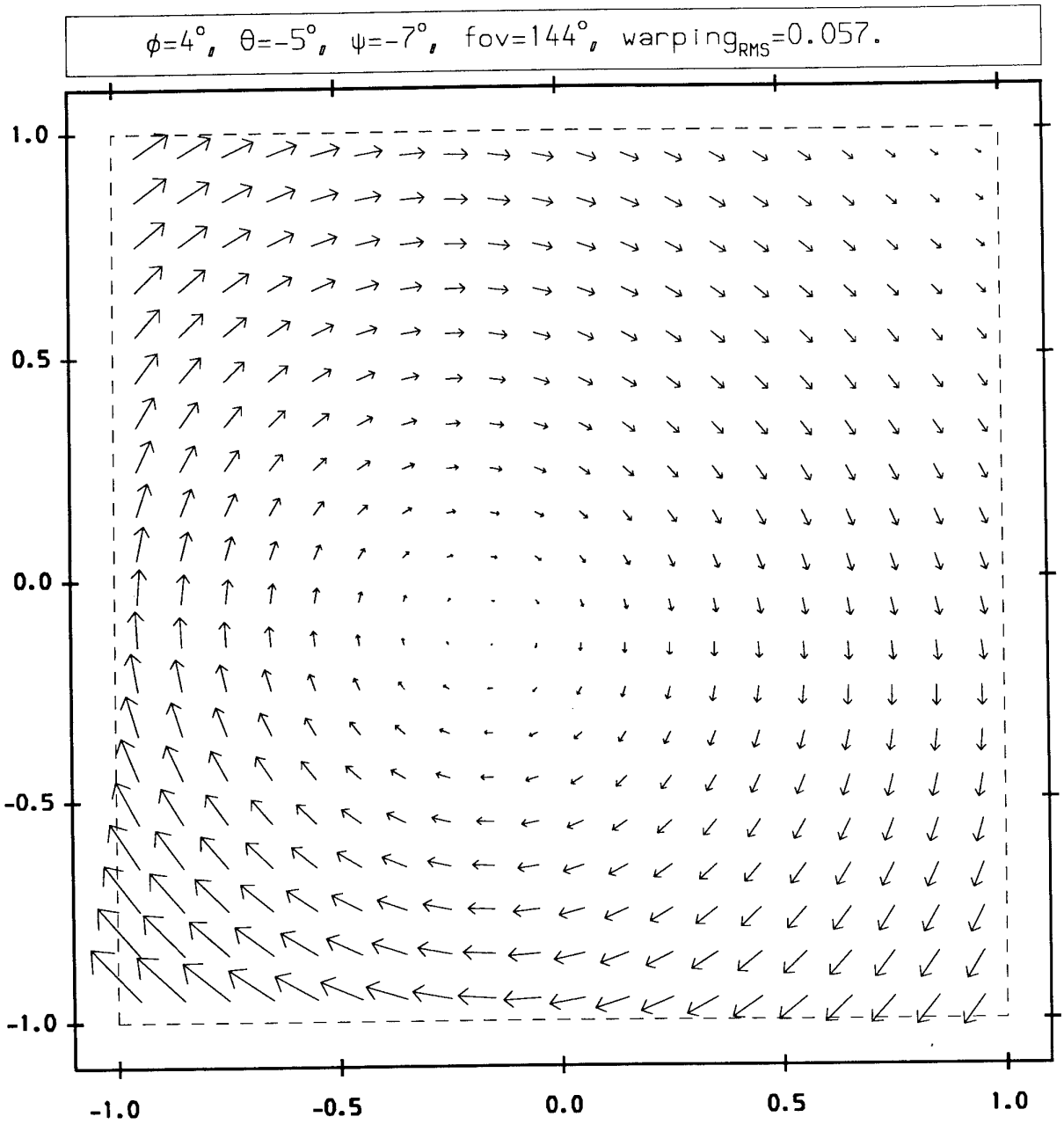

Figure 4: Geometric warping vector field (g_x, g_y) for the imaging characteristic of Figure 2, the indicated field of view, and camera rotation according to the indicated Euler angles. The displayed geometric warping excludes a global image translation component of $(0.09, -0.12)$ units. The root mean square value of the geometric warping also is indicated.

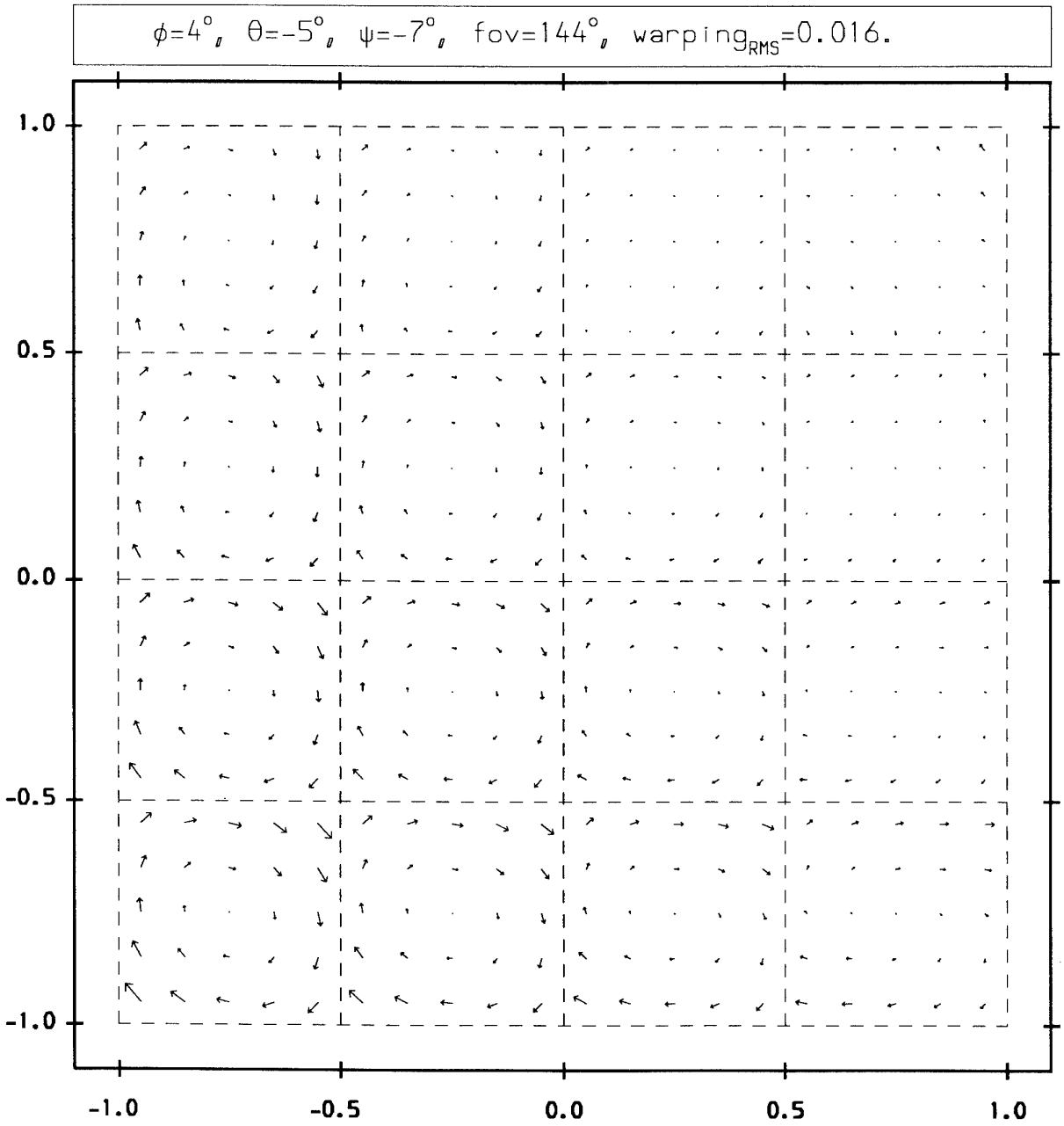

Figure 5: Geometric warping vector field (g_x, g_y) for the imaging characteristic of Figure 2, the indicated field of view, and camera rotation according to the indicated Euler angles. The image is partitioned into 4×4 subimages, each of which has its own particular translation excluded from the displayed geometric warping. The root mean square value of the geometric warping also is indicated. Compare with Figure 4.

conveyed by comparing the root mean square geometric warping values: $g_{\text{RMS}} = 0.057$ for the unsegmented image, and $g_{\text{RMS}} = 0.016$ for the segmented image. Inspection of Figure 5 suggests that the geometric warping in individual image segments may be significantly diminished by also correcting for image segment rotation. Thus, at least for this example, the intrinsic (non-shape-preserving) geometric warping for the segmented image is much smaller than that for the unsegmented image.

6 Radiometric warping due to optical system rotation

In contrast to geometric warping, radiometric warping seems to attract relatively little attention in the imaging science research literature. To some extent this neglect is justifiable. Many applications, such as navigation of, or manipulation by, robots, only require knowledge of the displacement of image points as the camera moves, to infer the changing disposition of object space with respect to the camera. The fact that the intensities of the image points conjugate to a given object point change over time is immaterial. Even if radiometric warping is important in principle, such as for addition or subtraction of images, it will be verified below that radiometric warping becomes significant only at larger field angles ($\theta \gtrsim 20°$). Since many imaging systems have a relatively narrow field of view ($2\theta_{\text{max}} \lesssim 20°$), the influence of radiometric warping on images often is marginal. Indeed, in such a case the intensity variations between images may be predominantly due to temporal noise and focal plane detection nonuniformity, rather than radiometric warping. However, this report specifically considers wide field of view imaging, in which case radiometric warping may be significant, as will be demonstrated below.

One construes from (21) that radiometric warping is the intensity ratio of final and initial image plane points that are conjugate to the same object space point. In the case of pure camera rotation, where the optical path from the object point to the entrance pupil of the camera is invariant, atmospheric nonuniformity and range variation can have no influence on the radiometric warping. Rather, the physical causes of radiometric warping (and indeed, distortion) are all due to variations with field angle of both the radiant energy flux propagating through the optical system, and the distribution of this flux on the focal plane. One is cautioned that the term 'radiometric distortion' is sometimes used by remote sensing researchers to describe the manifestations of changing optical path through the atmosphere, or temporal changes in the propagation of light along a given optical path. Other researchers define radiometric distortion to be the variation of detector sensitivity over the focal plane. Both of these usages are quite distinct from the ones adopted in this report for either distortion or warping.

For any differential element of area on the image plane, one seeks the conjugate element of area on the surface of the object (eg. the ground). Consider an infinitesimal annular arc in the image plane, with centre of curvature at the origin and position (ρ, α) expressed in plane polar coordinates (refer to Figure 6). The area of this differential element of image plane is,

$$\mathrm{d}a = \rho \, \mathrm{d}\alpha \, \mathrm{d}\rho \ . \tag{37}$$

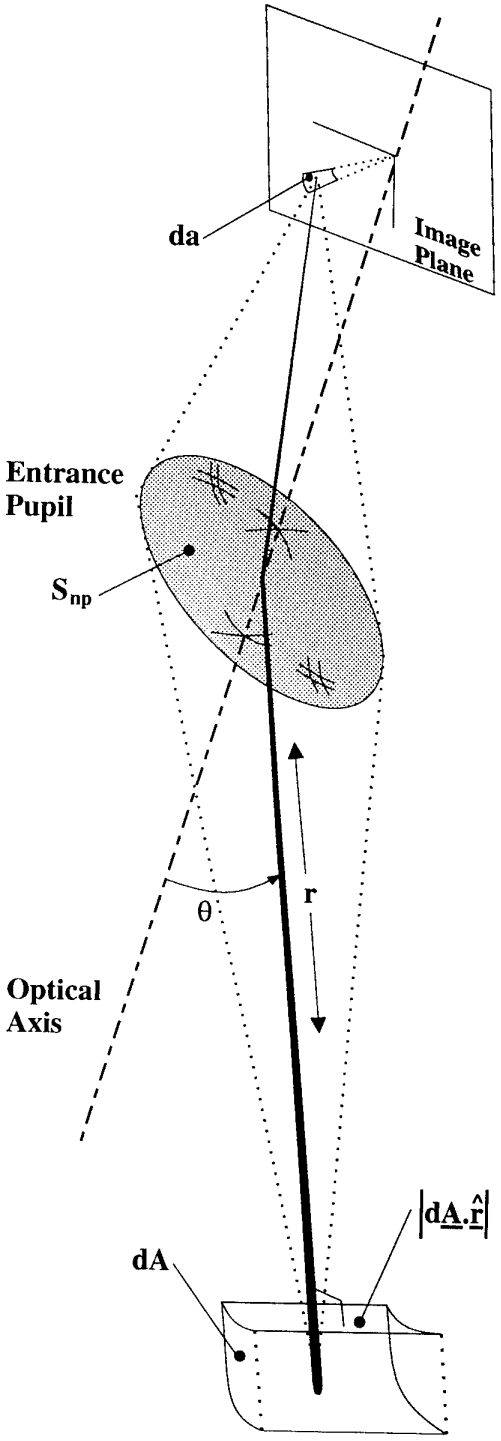

Figure 6: Conjugate differential elements of area in the image plane (da)*, and on the surface of the object* (dA)*.* $|d\mathbf{A}\cdot\hat{\mathbf{r}}|$ *is the magnitude of the projection of the element of object surface area along the radial direction.* S_{np} *is the area of the entrance pupil of the optical system; in general* S_{np} *depends on field angle* θ*. The chief ray is shown tapered, and the marginal rays by dotted lines.*

Substituting terms depending on only the object space polar and azimuthal angles (θ, ϕ) for terms on the right side of (37), according to (1) and (2), one obtains the relation,

$$\mathrm{d}\theta\,\mathrm{d}\phi = \frac{\mathrm{d}a}{F(\theta)\,F'(\theta)} \quad , \quad \text{where} \quad F'(\theta) \equiv \frac{\mathrm{d}F}{\mathrm{d}\theta} \quad . \tag{38}$$

$\mathrm{d}\theta$ and $\mathrm{d}\phi$ are both assumed to be positive without loss of generality. The element of solid angle in object space that is conjugate to $\mathrm{d}a$ in the image plane is,

$$\mathrm{d}\Omega = \sin\theta\,\mathrm{d}\theta\,\mathrm{d}\phi \quad , \tag{39}$$

which, upon substitution of (38), becomes,

$$\mathrm{d}\Omega = \frac{\sin\theta\,\mathrm{d}a}{F(\theta)\,F'(\theta)} \quad . \tag{40}$$

Let the object surface at angular position (θ, ϕ) be at distance r from the origin (ie. centre of the entrance pupil); spherical polar coordinates thus being (r, θ, ϕ). If $\mathrm{d}\mathbf{A}$ is the differential element of directed area on the object surface that is conjugate to $\mathrm{d}a$ in the image plane, then the projection of $\mathrm{d}\mathbf{A}$ along the radial direction $\hat{\mathbf{r}}$ is (refer to Figure 6),

$$\mathrm{d}\mathbf{A}\cdot\hat{\mathbf{r}} = -r^2\,\mathrm{d}\Omega \quad , \tag{41}$$

where the negative sign reflects the fact that if the element of object surface is visible from the origin, then the projection of its outward normal along the radial direction must be towards the origin. Substitution of (40) into (41) yields,

$$\mathrm{d}\mathbf{A}\cdot\hat{\mathbf{r}} = -\frac{r^2\,\sin\theta\,\mathrm{d}a}{F(\theta)\,F'(\theta)} \quad . \tag{42}$$

It is noteworthy that this analysis is valid for a general object surface topography; the object surface is not constrained to be planar. This generality is maintained for the remainder of the analysis, despite other restrictions being imposed to facilitate analytical development.

One seeks the radiant flux that is emitted, scattered or reflected from object surface element $\mathrm{d}A$ and is incident upon its conjugate image plane surface element $\mathrm{d}a$, after propagation through the optical system. In this report the term 'emission' often will be interpreted as also encompassing scattering and reflection.

For radiation collection purposes, the optical system is entirely represented by its entrance pupil. However, for a general axially symmetrical optical system, the shape, area, position and orientation of the entrance pupil all vary with field angle θ; even in the absence of vignetting. This phenomenon is demonstrated for a fish eye lens, with internal aperture stop, by Kingslake [6, p. 87,88]. The influence of entrance and exit pupils on the illumination properties of optical systems has been elucidated by the careful analyses of Reiss [16, 17], Slussareff [18] and Gardner [19]. The presence of vignetting effectively causes the entrance pupil to vary even more rapidly with field angle; in particular, the entrance pupil area diminishes much more rapidly with increasing θ. Aspects of vignetting in wide field of view optical systems have been studied by Sands [20].

To account properly for the variation of the entrance pupil with field angle for a general optical system is a formidable undertaking, and in some respects, a digression from the main theme of this report. Accordingly, to facilitate the present analysis, the directed area of the entrance pupil will be assumed to have the constant value $S_{\rm np}$ along the optical axis at all field angles θ. An optical system with this property is conceivable: any optical system that has a sufficiently small diaphragm in front of all lens elements, small enough that the diaphragm remains the aperture stop at all field angles, with all lens elements having sufficiently wide clear apertures to prevent vignetting at all field angles. It is emphasised that it is not sufficient for the entrance pupil to be in front of all lens elements; the physical aperture stop must also be so positioned. Such an optical system has its entrance pupil coinciding with its aperture stop. Consequently, since the aperture stop is a mechanical entity, it follows that there is no scope for the entrance pupil to vary with field angle.

One is cautioned that most wide field imaging systems do not conform to this prescription, due to one or more of the following reasons: the presence of an internal aperture stop, different diaphragms assuming the role of aperture stop in different field angle intervals, and the presence of vignetting. Nevertheless, optical systems which are not afflicted by at least some of these 'problems' have been devised. The fish eye lens discussed by Kingslake [6, p. 87,88] maintains the same (internal) aperture stop at all field angles, and it is never subject to vignetting, not even at large field angles. Wide field of view lenses with the aperture stop positioned in front of all lens elements have been designed by Dudragne [21] and Yasukuni [22]. The analytical expressions for radiometric distortion and warping that will be derived in this section will admittedly only pertain to an idealised, hypothetical, but conceivable, optical system; but the underlying reasoning leading to its derivation is precisely that which would have to be invoked for any practical optical system.

One infers from Figure 6, that the solid angle subtended by the entrance pupil at a distant object point with spherical polar coordinates (r, θ, ϕ) is,

$$\Omega_{\rm np} = \frac{S_{\rm np}\,\cos\theta}{r^2} \quad . \tag{43}$$

Equation (43) assumes that the object point distance r is sufficiently large for the marginal rays to be parallel to the chief ray, or equivalently, that the radius of the entrance pupil is much smaller than r. Under any practical conditions, this assumption definitely is valid. The radiant flux emanating from object surface element $\mathrm{d}A$ that is collected by the optical system is,

$$\mathrm{d}\Phi_e = L_e(\mathbf{x}, -\hat{\mathbf{r}})\,[\mathrm{d}\mathbf{A}\cdot -\hat{\mathbf{r}}]\,\Omega_{\rm np} \quad , \tag{44}$$

where $L_e(\mathbf{x}, -\hat{\mathbf{r}})$ is the radiance of the object surface at surface location $\mathbf{x}$ and in direction $-\hat{\mathbf{r}}$ (recall that $\hat{\mathbf{r}}$ is the unit vector from the centre of the entrance pupil to the object point).

Neglecting the occurrence of absorption, scattering and reflection of light within the optical system, all of the radiant flux $\mathrm{d}\Phi_e$ impinges upon the image plane area that is conjugate to $\mathrm{d}A$, that is, $\mathrm{d}a$ of (37), as illustrated in Figure 6. The image plane irradiance E_e, which is the most appropriate measure of image intensity s, becomes by (44),

$$s = E_e \equiv \frac{\mathrm{d}\Phi_e}{\mathrm{d}a} = L_e(\mathbf{x}, -\hat{\mathbf{r}})\,\frac{\mathrm{d}\mathbf{A}\cdot -\hat{\mathbf{r}}}{\mathrm{d}a}\,\Omega_{\rm np} \quad , \tag{45}$$

which, upon substitution of (42) and (43), becomes for an object point at infinity,

$$E_e = \frac{1}{2} S_{\rm np}\, L_e(\mathbf{x}, -\hat{\mathbf{r}})\, \frac{\sin 2\theta}{F(\theta)\, F'(\theta)} \quad . \tag{46}$$

Inspection of (46) reveals that the image plane irradiance is independent of the object distance, as long as that distance is large. This behaviour is due to the combination of an r^2 dependence of the element of object surface area conjugate to a given image plane area, and an inverse r^2 dependence of the solid angle subtended by the entrance pupil at the object point. An optical system that exhibits no distortion aberration has the imaging characteristic (3), for which (46) yields the image plane irradiance variation,

$$E_e = \frac{S_{\rm np}\, L_e(\mathbf{x}, -\hat{\mathbf{r}})}{f^2} \cos^4\theta \qquad \text{(perfect imaging)} \quad . \tag{47}$$

Thus, a 'perfect' imaging system has no geometric distortion, but it does have the radiometric distortion of (47). If the geometric distortion is described by imaging characteristic (4), then the image plane irradiance varies as,

$$E_e = \frac{S_{\rm np}\, L_e(\mathbf{x}, -\hat{\mathbf{r}})}{f^2} \frac{\sin 2\theta}{2\theta} \qquad \text{(actual imaging)} \quad , \tag{48}$$

indicating the presence of radiometric distortion. In (47) and (48), θ is the angle between the object point and optical axis measured at the centre of the entrance pupil. Both (47) and (48) are consistent with a contention of the opening paragraph of this section—that radiometric distortion and warping only tend to become significant at larger field angles.

Expression (46) for the irradiance variation over the image plane has been previously derived by Reiss [17] and Kingslake [23, Section 5.III.7], for the more restricted case of a planar object surface oriented normally to the optical axis. The present derivation is much simpler, although it is not amenable to generalisation to the case of a varying entrance pupil with obliquity (which would be the situation for a non-frontal aperture stop or vignetting), nor to a finite object distance. Such generalisations are encapsulated in the formal analyses of Reiss [16, 17], Slussareff [18] and Gardner [19]. The present derivation is distinguished by the absence of any assumption about the topography of the object surface (provided it remains at infinity everywhere); hence the image plane irradiance variation (46) has validity beyond the planar object surface normal to the optical axis that has been assumed in previous derivations. It is important to establish this applicability to all object surface topographies, since if the object is a realistic landscape, it will have very many inclined facets.

One is now able to express the radiometric warping $R(x_0, y_0)$ defined by (21) in terms of the imaging characteristic and the common object point polar angles before and after displacement of the optical system:

$$R(x_0, y_0) \equiv \frac{s_1(x_1, y_1)}{s_0(x_0, y_0)} = \frac{E_{e1}(x_1, y_1)}{E_{e0}(x_0, y_0)} \quad . \tag{49}$$

Since (x_1, y_1) is determined from (x_0, y_0) according to the geometric transformation, the radiometric warping is a scalar field in the initial image plane. Substituting (46) into (49)

yields the desired expression for radiometric warping within the infinite object distance approximation,

$$R(x_0, y_0) = \frac{L_e(\mathbf{x}, -\hat{\mathbf{r}}_1)\, \sin 2\theta_1\, F(\theta_0)\, F'(\theta_0)}{L_e(\mathbf{x}, -\hat{\mathbf{r}}_0)\, \sin 2\theta_0\, F(\theta_1)\, F'(\theta_1)} \quad , \tag{50}$$

where the 0/1 subscript signifies quantities measured with respect to the initial/final coordinate system (frame O_0/O_1).

For the present, restrict the optical system displacement to be pure rotation, as done in Section 5. Since $\hat{\mathbf{r}}$ specifies the direction from the centre of the entrance pupil to the object point, neither of which are displaced in the 'world' coordinate system, one has,

$$\hat{\mathbf{r}}_1 = \hat{\mathbf{r}}_0 \qquad \text{(pure rotation)} \quad , \tag{51}$$

in which case (50) simplifies to,

$$R(x_0, y_0) = \frac{\sin 2\theta_1\, F(\theta_0)\, F'(\theta_0)}{\sin 2\theta_0\, F(\theta_1)\, F'(\theta_1)} \qquad \text{(pure rotation)} \quad . \tag{52}$$

The initial and final field angles are determined by the geometric warping evaluation algorithm of Section 5; θ_0 emerging at (23) in the algorithm, and θ_1 emerging at (27). Inspection of (52) confirms that the radiometric warping $R(x_0, y_0)$ does not depend on the illumination conditions, or the reflection, scattering and emission properties of the object surface, in any way. This verifies the contention of Section 4 for the case of pure rotation. Furthermore, since it has been determined in Section 5 that the mapping of θ_0 to θ_1 is not influenced by the ground topography, it follows from (52) that the radiometric warping is also completely independent of the ground topography, for pure rotation.

As done for geometric warping in Section 5, it is most appropriate to introduce the *intrinsic* radiometric warping scalar field,

$$R_{\text{in}}(x_0, y_0) \equiv \frac{s_1(x_1, y_1) - u s_0(x_0, y_0)}{u s_0(x_0, y_0)} \quad , \tag{53}$$

where constant parameter u is to be optimally chosen as indicated below. The intrinsic radiometric warping vanishes if the final image amplitudes are everywhere the same multiple u of the initial image amplitudes, where the initial and final image points are related by the geometric transformation. This is a desirable property, since uniform scaling of initial image amplitudes to obtain final image amplitudes does not constitute a radiometric warping in the colloquial sense. Substituting definition (49) into definition (53) yields,

$$R_{\text{in}}(x_0, y_0) = \frac{1}{u} R(x_0, y_0) - 1 \quad . \tag{54}$$

The root mean square intrinsic radiometric warping is,

$$\begin{aligned} R_{\text{in}_{\text{RMS}}}(u) &\equiv \left(\frac{1}{\text{Area}} \iint\limits_{\substack{\text{complete} \\ \text{image}}} R_{\text{in}}^2(x_0, y_0)\, \mathrm{d}x_0\, \mathrm{d}y_0 \right)^{1/2} \quad , \\ &= \left(\frac{1}{\text{Area}} \iint\limits_{\substack{\text{complete} \\ \text{image}}} \left(\frac{1}{u} R(x_0, y_0) - 1 \right)^2 \mathrm{d}x_0\, \mathrm{d}y_0 \right)^{1/2} \quad . \end{aligned} \tag{55}$$

Parameter u is optimised according to the least squares criterion,

$$\underset{u}{\text{minimum}}\ R_{\text{in}_{\text{RMS}}}(u) \ , \tag{56}$$

whose solution is the optimum uniform scaling for the initial image amplitude,

$$\widehat{u} \ = \iint\limits_{\substack{\text{complete}\\ \text{image}}} R^2(x_0, y_0)\ \mathrm{d}x_0\ \mathrm{d}y_0 \Big/ \iint\limits_{\substack{\text{complete}\\ \text{image}}} R(x_0, y_0)\ \mathrm{d}x_0\ \mathrm{d}y_0 \ , \tag{57}$$

where the numerator and denominator are both (almost) certainly non-zero, since the non-negative nature of image intensity ensures that $R(x_0, y_0) \geq 0$ everywhere. The severity of the intrinsic radiometric warping may be quantified by the minimum of its root mean square value, that is, by $R_{\text{in}_{\text{RMS}}}(\widehat{u})$.

Figure 7 illustrates the intrinsic radiometric warping scalar field $R_{\text{in}}(x_0, y_0)$ for identical optics and rotation parameters as the example introduced in Section 5; it is associated with the geometric warping vector field graphed in Figure 4. Since this example corresponds to pure camera rotation, the intrinsic radiometric warping scalar field is completely independent of the actual scene and its topography. The initial image is uniformly scaled by the factor $\widehat{u} = 1.0067$, and the ensuing root mean square intrinsic radiometric warping is $R_{\text{in}_{\text{RMS}}} = 0.135$ units. Inspection of Figure 7 verifies that the intrinsic radiometric warping is most extreme on some portions of the periphery of the field of view, although not everywhere on the periphery.

Repeating the image segmentation exercise of Section 5 results in the intrinsic radiometric warping scalar field illustrated in Figure 8, in which a separate uniform scale factor is applied to each initial image segment. The associated geometric warping vector field is the one graphed in Figure 5. Apart from the fact that different segments in Figure 8 have different optimal initial image scalings, the radiometric warping fields of Figures 7 and 8 are otherwise identical. As for geometric warping, one confirms that the severity of radiometric warping is reduced significantly by operating on small image segments: $R_{\text{in}_{\text{RMS}}} = 0.135$ for the unsegmented image, and $R_{\text{in}_{\text{RMS}}} = 0.042$ for the segmented image. However, Figure 8 indicates that the intrinsic radiometric warping of some image segments, in particular the one centred at $(0.75, -0.75)$, is still quite substantial. This would serve to frustrate subimage registration by cross correlation; a more sophisticated technique may be necessary.

7 Image warping due to arbitrary optical system displacement

Sections 5 and 6 addressed the geometric and radiometric image warping resulting from pure rotation of the camera. However, an arbitrary rigid body displacement is resolvable into two operations (Chasles' theorem; Goldstein [11, Sec. 4-6]): rotation about a centre, and displacement of that centre (ie. translation). In this section, one examines

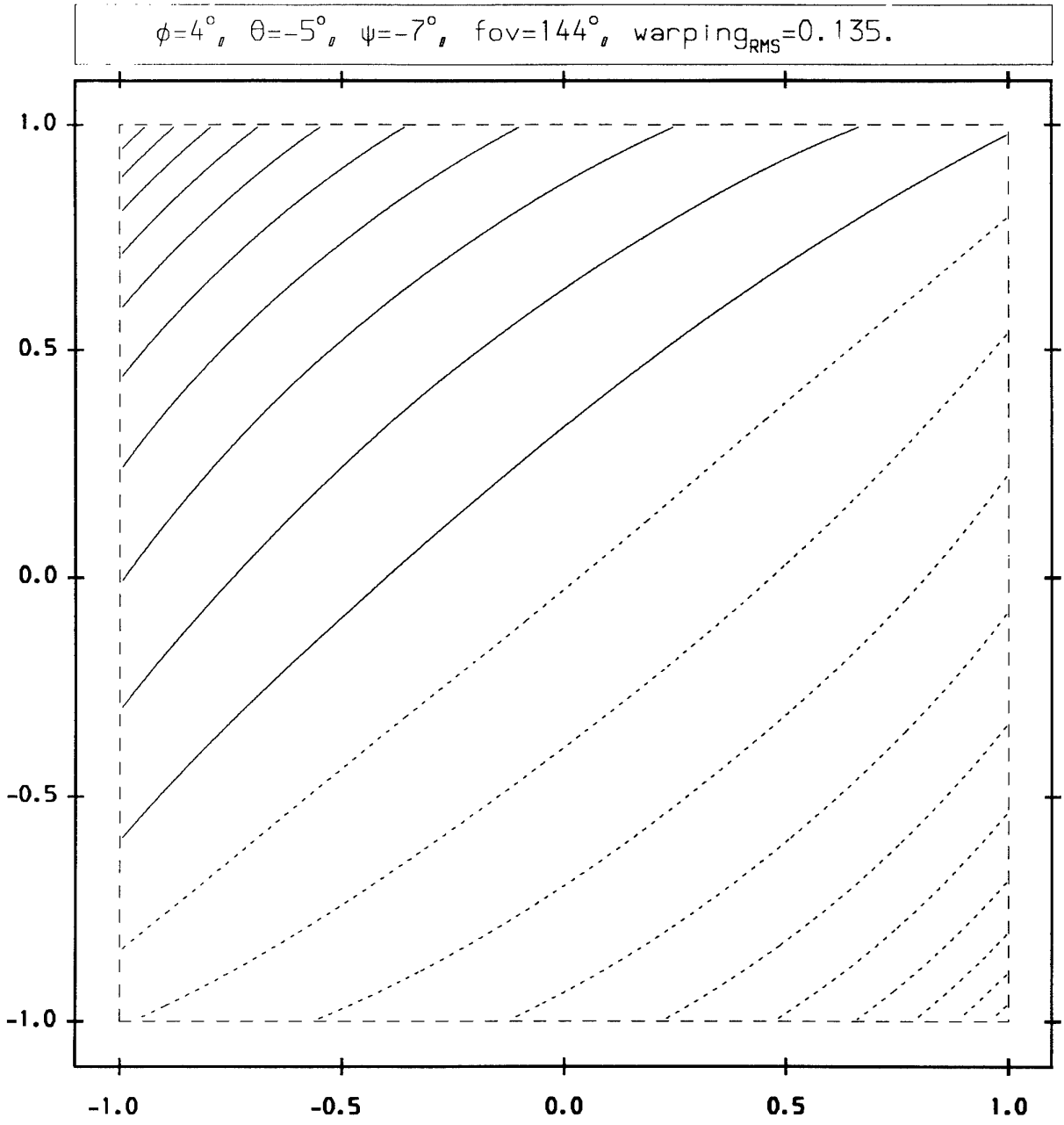

Figure 7: Intrinsic radiometric warping scalar field $R_{\text{in}}(x_0, y_0)$ in the initial image plane, for the imaging characteristic of Figure 2, the indicated field of view, and camera rotation according to the indicated Euler angles. The initial image amplitude is uniformly scaled by the factor 1.0067. Contour spacing is ΔR_{in}=0.050 units, symmetrically disposed about R_{in}=0, with negative values indicated by broken lines and positive values by continuous lines. Contour values increase monotonically as one progresses from $(1, -1)$ to $(-1, 1)$. The root mean square value of the intrinsic radiometric warping also is indicated.

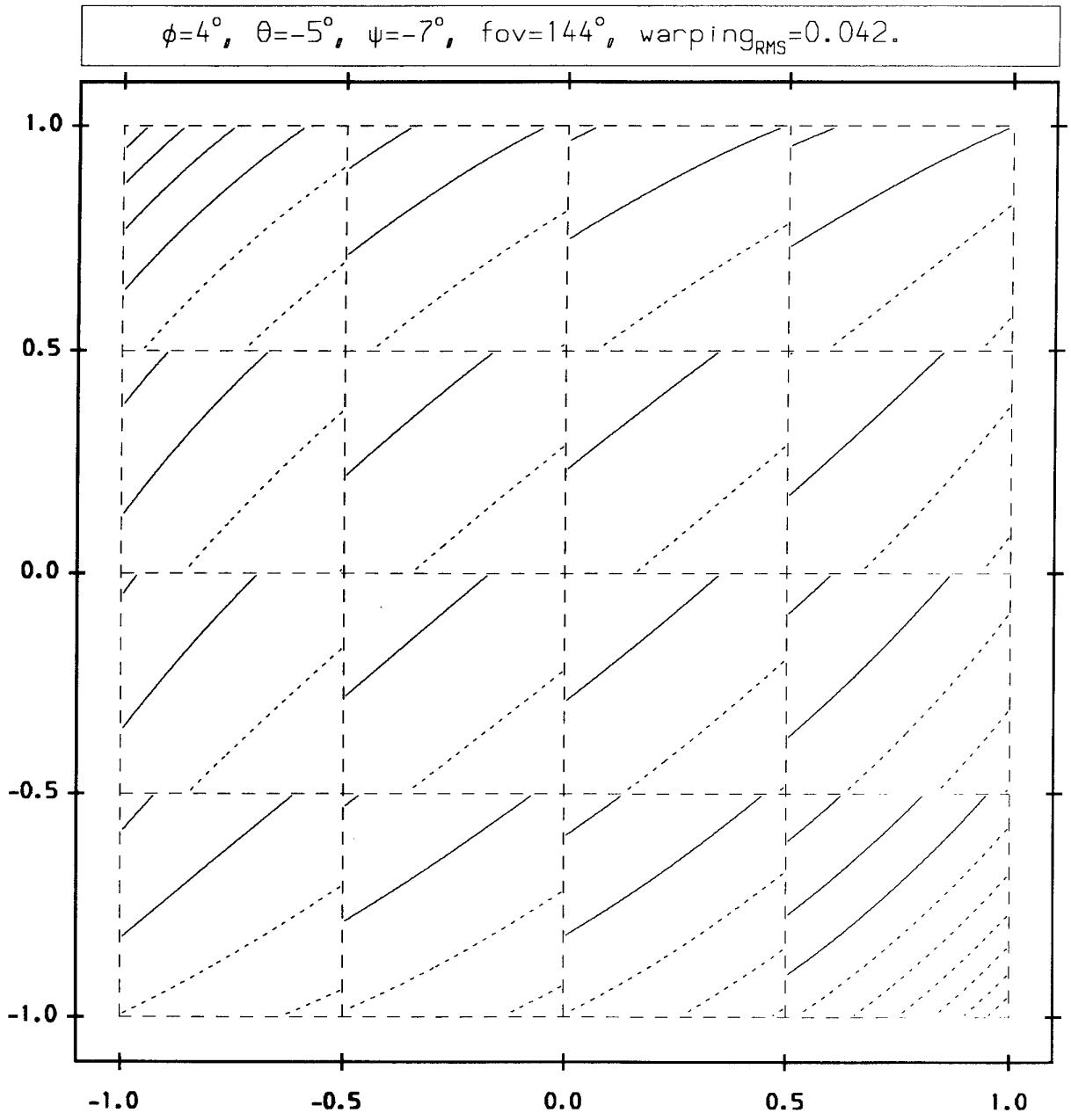

*Figure 8: **Intrinsic radiometric warping scalar field** $R_{\text{in}}(x_0, y_0)$ in the initial image plane, for the imaging characteristic of Figure 2, the indicated field of view, and camera rotation according to the indicated Euler angles. The image is partitioned into 4×4 subimages, each of which is corrected for its own particular mutual scaling between initial and final images. The root mean square value of the intrinsic radiometric warping also is indicated. Compare with Figure 7, with which this graph shares the same contouring scheme.*

how the preceding analysis is modified to account for the arbitrary translation vector **b** from the initial to the final centre of the entrance pupil, in addition to the camera rotation. The consequences of the inclusion of camera translation will be elucidated, although no computational results will be presented.

Translation vector **b** has cartesian coordinates (b_x, b_y, b_z) in the cardinal reference frame O introduced in Section 3. The geometric warping algorithm remains essentially as in Section 5, subject to the extension of (26) to become,

$$\begin{bmatrix} x'_1 \\ y'_1 \\ z'_1 \end{bmatrix} = \mathbf{T}_{01} \begin{bmatrix} x'_0 \\ y'_0 \\ z'_0 \end{bmatrix} - \mathbf{T}_1 \begin{bmatrix} b_x \\ b_y \\ b_z \end{bmatrix} , \tag{58}$$

where $\mathbf{T}_1$ is the rotation matrix from frame O to frame O_1, as in (16).

Since (58) is not an orthogonal transformation, because of the translation term, the radial distance of the invariant object point from the centre of the entrance pupil changes with camera displacement, that is,

$$r_1 \neq r_0 = r \qquad \text{(translation and rotation)} , \tag{59}$$

in contrast to (28) for pure rotation. More importantly, the direction of the object point in frame O_1, as expressed by angles θ_1 and ϕ_1 of (27), now does depend on r. Consequently, the final image plane point that emerges in Step 4 of the geometric warping algorithm now does depend on r. This implies that for general camera displacement, the association of an initial image plane point with a final image plane point (ie. the geometric warping) formally depends on the topography of the object surface (eg. ground).

In Section 6 the direction of the invariant object point from the centre of the entrance pupil is denoted by $\hat{\mathbf{r}}$; since the centre of the entrance pupil now undergoes a displacement, this direction changes between reference frames O_0 and O_1, that is,

$$\hat{\mathbf{r}}_1 \neq \hat{\mathbf{r}}_0 \qquad \text{(translation and rotation)} , \tag{60}$$

in contrast to (51) for pure rotation. Therefore, for general object surface radiance $L_e(\mathbf{x}, -\hat{\mathbf{r}})$, the radiometric warping no longer simplifies from (50) to (52) in the presence of camera translation. Inspection of (50) reveals that for general camera displacement and object radiance, the radiometric warping depends on the anisotropy of emission/scattering/reflection from the object surface, this anisotropy in part being due to illumination conditions. Such behaviour is contrary to the assertion of Section 4, which is now recognised as not being a universal principle.

An ideal Lambertian, or diffuse, source, is a perfectly isotropic emitter, for which the radiance is independent of direction, that is,

$$L_e(\mathbf{x}, -\hat{\mathbf{r}}_1) = L_e(\mathbf{x}, -\hat{\mathbf{r}}_0) = L_e(\mathbf{x}) \qquad \text{(Lambertian source)} . \tag{61}$$

If the object surface is a Lambertian emitter, the radiometric warping once again simplifies from (50) to (52); this time for arbitrary camera displacement. Thus, one has,

$$R(x_0, y_0) = \frac{\sin 2\theta_1 \, F(\theta_0) \, F'(\theta_0)}{\sin 2\theta_0 \, F(\theta_1) \, F'(\theta_1)} \qquad \begin{matrix} \text{(Lambertian source;} \\ \text{translation and rotation)} \end{matrix} , \tag{62}$$

and one concludes that a Lambertian object surface gives rise to a radiometric warping that is independent of the directionality of the illumination, and the unconstrained reflection, scattering and emission characteristics of the surface, for an arbitrary camera displacement. The radiometric warping resulting from a Lambertian object surface and arbitrary camera displacement is once again consistent with the assertion of Section 4.

Whether the radiometric warping is described by (50) or (62), it depends on the mapping between θ_0 and θ_1. It has been established in this section that this mapping is influenced by the ground topography in the presence of camera translation. Consequently, the radiometric warping implicitly depends on the ground topography for general camera displacement, even for Lambertian emission; Lambertian emission only removes the dependence of the radiometric warping on the (isotropic) radiance of the surface.

8 Conclusions

It is conceptually appealing to decompose the image warping arising from an optical system displacement into geometric and radiometric components, and consider them separately, as has been done in this report. However, ultimately the two components combine according to (20) and (21) to yield the complete initial to final image transformation. Schemes for approximating the geometric and radiometric transformations may be devised. For example, one may approximate the functions $X_{01}(x_0, y_0)$, $Y_{01}(x_0, y_0)$ and $R(x_0, y_0)$ of Section 4 by polynomials of specified orders; which may be chosen, among other ways, by truncating the power series expansion of the exact functions beyond a certain number of terms.

The ultimate arbiter of the fidelity of the approximations is the discrepancy between the transformed images arising from approximate and exact complete transformations applied to the same initial imge. This discrepancy can not easily be ascertained by individual consideration of the geometric and radiometric components in isolation; the two transformation components operate synergistically in warping the image. Furthermore, the discrepancy between transformed images depends upon the initial image to which the transformations are applied, even though the transformations themselves are image invariant (for pure rotation).

Although g_{RMS} (36) and $R_{\mathrm{in}_{\mathrm{RMS}}}$ (55) are quantitative measures of geometric and radiometric warping, the most meaningful measure would actually be the root mean square image difference (appropriately normalised). However, unlike g_{RMS} and $R_{\mathrm{in}_{\mathrm{RMS}}}$, the value of this metric depends on the image content as well as the warping between initial and final images. Different object space distributions give different warping measures. The most representative single measure of warping in this case would be an ensemble average of the warping measure for all possible object distributions of interest. Such an ensemble average would only depend on the warping between initial and final images.

The ensemble averaging procedure in principle requires the availability of a large ensemble of representative background images. Equivalently, one can use a valid statistical model of the background random field, in which case all ensemble averages are deducible from the joint probability density function.

This report has elucidated the exact solution to the problem of image registration that arises as a result of displacement of an idealised optical system, and it is quite reasonable to expect that the qualitative features of the solution also apply to any practical imaging system. These results have immediate practical utility to the problem that inspired the research—airborne passive missile detection by differential motion observation, as reported by Caprari [1]. Simulations of the magnitude of observed differential motion of missiles relative to the background, as presented in [1], indicate that differential motion is quite small compared with the image resolution (i.e. pixel size) and absolute motion of the whole image (due to aircraft motion). This circumstance emphasises the critical importance of achieving precision in the image registration step of the differential motion determination. Research presented in this report forms the theoretical foundation upon which a practical precision image registration system would need to be based.

An incidental, but important, result of this research is the demonstration of the severity of the radiometric distortion towards the perimeter of a wide field image. A practical implication of this, is that any image processing algorithm that utilises image intensity thresholding, would need to use local threshold values to achieve equally reliable operation across the complete image.

Acknowledgements

The author expresses his gratitude to Warwick Holen for assisting in the drafting of Figures 1, 3 and 6; and Derek Bertilone, Chris Woodruff and Garry Newsam for their constructive criticism of preliminary drafts of this report. This research has been funded by Land, Space and Optoelectronics Division of Defence Science and Technology Organisation. Facilities made available to the author by Flinders University, courtesy of the Department of Physics, assisted in the conduct of this research and the drafting of this report.

Appendix A

Transformation of polar coordinates due to rotation of reference frame

In Section 5 the geometric transformation due to optical system rotation was expressed as a four step algorithm. An alternative, explicit solution of this problem will be presented here without derivation. For brevity of expression, what is presented is the geometric transformation from object point polar coordinates (r_0, θ_0, ϕ_0) in initial frame O_0, to polar coordinates (r_1, θ_1, ϕ_1) of the same object point in rotated frame O_1. To complete the image plane to image plane geometric transformation, one only needs to include the simple relationships between object space polar coordinates and image plane cartesian coordinates that are stated in Section 5—being (22) and (23), and its inverse, (29) and (31).

Denote the elements of the rotation matrix from O_0 to O_1 by t_{ij}, $i, j = 1, 2, 3$. Then the axis of rotation (in either frame O_0 or O_1) is the vector

$$\mathbf{n}' = \begin{bmatrix} t_{12}t_{31} - t_{13}t_{21} \\ (1 - t_{11})(t_{31} - t_{13}) \\ (1 - t_{11})(t_{12} - t_{21}) \end{bmatrix} , \tag{A1}$$

and the unit vector in the direction of the rotation axis is

$$\mathbf{n} \equiv \begin{bmatrix} n_1 \\ n_2 \\ n_3 \end{bmatrix} = \frac{\mathbf{n}'}{\|\mathbf{n}'\|} . \tag{A2}$$

The angle of rotation of the coordinate system about axis $\mathbf{n}$ is

$$\Omega = \arccos\left(\frac{t_{11} + t_{22} + t_{33} - 1}{2}\right) \quad \Omega \in [0, \pi] . \tag{A3}$$

Finally, the polar coordinate transformation from initial frame O_0 to rotated frame O_1 is

$$\begin{aligned} r_1 &= r_0 , \\ \theta_1 &= \arccos[n_3(n_1 \sin\theta_0 \cos\phi_0 + n_2 \sin\theta_0 \sin\phi_0 + n_3 \cos\theta_0)(1 - \cos\Omega) + \\ &\qquad (n_2 \sin\theta_0 \cos\phi_0 - n_1 \sin\theta_0 \sin\phi_0) \sin\Omega + \cos\theta_0 \cos\Omega] \quad \theta_1 \in [0, \pi] , \\ \phi_1 &= \arctan\left[\frac{\begin{array}{l} n_2(n_1 \sin\theta_0 \cos\phi_0 + n_2 \sin\theta_0 \sin\phi_0 + n_3 \cos\theta_0)(1 - \cos\Omega) + \\ (n_1 \cos\theta_0 - n_3 \sin\theta_0 \cos\phi_0) \sin\Omega + \sin\theta_0 \sin\phi_0 \cos\Omega \end{array}}{\begin{array}{l} n_1(n_1 \sin\theta_0 \cos\phi_0 + n_2 \sin\theta_0 \sin\phi_0 + n_3 \cos\theta_0)(1 - \cos\Omega) + \\ (n_3 \sin\theta_0 \sin\phi_0 - n_2 \cos\theta_0) \sin\Omega + \sin\theta_0 \cos\phi_0 \cos\Omega \end{array}}\right] \end{aligned} \tag{A4}$$

(quadrant determined by signs of numerator and denominator) .

References

1. R. S. Caprari, "Missile detection by observation of differential motion in an image sequence", DSTO Research Report DSTO-RR-0018, October 1995.

2. J. R. G. Townshend, C. O. Justice, C. Gurney and J. McManus, "The impact of misregistration on change detection", IEEE Trans. Geosci. Remote Sensing **30**, 1054–1060 (1992).

3. B. E. Bonshtedt, D. N. Eskov and A. J. Smirnov, "Stabilization of optical image in Earth's surveillance systems", Int. J. Imaging Sys. Technol. **4**, 65–68 (1992).

4. R. S. Caprari, "Geometric and radiometric image warping due to optical system displacement", Opt. Comm., accepted for publication (1997).

5. K. Miyamoto, "Fish eye lens", J. Opt. Soc. Am. **54**, 1060–1061 (1964).

6. R. Kingslake, *Optical System Design*, Academic Press, New York (1983).

7. I. C. Gardner and F. E. Washer, "Lenses of extremely wide angle for airplane mapping", J. Opt. Soc. Am. **38**, 421–431 (1948); Journal of Research of the National Bureau of Standards **40**, 93–103 (1948).

8. A. Kawamura, "Anamorphic $f\theta$ lens system", U.S. Patent 4277128 (1981).

9. B. Hayashida, "$F(\theta)$ lens system of four group construction", U.S. Patent 4400063 (1983).

10. S. Shah and J. K. Aggarwal, "A simple calibration procedure for fish eye (high distortion) lens camera", Proc. 1994 IEEE Int. Conf. Robotics and Automation—Vol. 4, IEEE Computer Society Press, Los Alamitos, Calif. (1994).

11. H. Goldstein, *Classical Mechanics*, 2nd ed., Addison-Wesley, Reading MA (1980).

12. J. Merchant, "Exact area registration of different views of a common object scene", Opt. Eng. **20**, 424–436 (1981).

13. B. K. P. Horn,"Relative orientation", Int. J. Comput. Vision **4**, 59–78 (1990).

14. B. K. P. Horn, "Relative orientation revisited", J. Opt. Soc. Am. A **8**, 1630–1638 (1991).

15. M. D. Pritt, "Automated subpixel image registration of remotely sensed imagery", IBM J. Res. Develop. **38**, 157–166 (1994).

16. M. Reiss, "The $\cos^4$ law of illumination", J. Opt. Soc. Am. **35**, 283–288 (1945).

17. M. Reiss, "Notes on the $\cos^4$ law of illumination", J. Opt. Soc. Am. **38**, 980–986 (1948).

18. G. Slussareff, "A reply to Max Reiss", J. Opt. Soc. Am. **36**, 707–707 (1946).

19. I. C. Gardner, "Validity of the cosine-fourth-power law of illumination", Journal of Research of the National Bureau of Standards **39**, 213–219 (1947).

20. P. J. Sands, "Prediction of vignetting", J. Opt. Soc. Am. **63**, 803–805 (1973).

21. R. A. Dudragne, "Wide-angle objective lens", U.S. Patent 3784286 (1974).

22. M. Yasukuni, "Lens system with frontal aperture stop", U.S. Patent 4093348 (1978).

23. R. Kingslake, "Illumination in optical images", Chapter 5 in *Applied Optics and Optical Engineering—Volume II*, R. Kingslake (ed.), Academic Press, NY (1965).

THIS PAGE IS INTENTIONALLY BLANK

Geometric and Radiometric Image Warping Due to Displacement of Wide Field Optical Systems

Robert S. Caprari

AUSTRALIA

1. DEFENCE ORGANISATION

a. HQ ADF
DSA (AIR)

b. S&T Program
Chief Defence Scientist
FAS Science Policy
AS Science Industry and External Relations
AS Science Corporate Management
} shared copy
Counsellor Defence Science, London (Doc Data Sheet)
Counsellor Defence Science, Washington (Doc Data Sheet)
Scientific Adviser to MRDC Thailand (Doc Data Sheet)
Director General Scientific Advisers and Trials
Scientific Adviser Policy and Command
Navy Scientific Adviser (3 copies Doc Data Sheet and one copy of the distribution list)
Scientific Adviser - Army (Doc Data Sheet and distribution list only)
Air Force Scientific Adviser
Director Trials

Electronics and Surveillance Research Laboratory
Director

Chief of Land Space and Opto-electronics Division
Research Leader, Space and Surveillance Systems, LSOD
Head, Image Processing Discipline
Dr D. Bertilone, LSOD
Dr V. Shettigara, LSOD
Mr R. Whatmough, LSOD
Dr R. Caprari, LSOD (2 copies)
Dr T. Payne, LSOD
Mr G. Hamlyn, LSOD
Research Leader, Electronic Countermeasures, EWD
Dr S. Brunker, EWD
Dr S. Kelly, EWD

Aeronautical and Maritime Research Laboratory
Director
Head, Advanced Seekers Group, WSD
Dr M. Wegener, WSD

DSTO Library
Library Fishermens Bend
Library Maribyrnong
Library DSTOS (2 copies)
Australian Archives

Library, MOD, Pyrmont (Doc Data sheet)

c. **Forces Executive**
Director General Force Development (Sea), (Doc Data Sheet)
Director General Force Development (Land), (Doc Data Sheet)
Director General Force Development (Air)

d. **Navy**
No compulsory distribution

e. **Army**
ABCA Office, G-1-34, Russell Offices, Canberra (4 copies)

f. **Air Force**
No compulsory distribution

g. **S&I Program**
Defence Intelligence Organisation
Library, Defence Signals Directorate (Doc Data Sheet only)

h. **Acquisition and Logistics Program**
No compulsory distribution

i. **B&M Program (libraries)**
OIC TRS, Defence Central Library
Officer in Charge, Document Exchange Centre (DEC), 1 copy
DEC requires the following copies of public release reports to meet exchange agreements under their management:
*US Defence Technical Information Center, 2 copies
*UK Defence Research Information Centre, 2 copies
*Canada Defence Scientific Information Service, 1 copy
*NZ Defence Information Centre, 1 copy
National Library of Australia, 1 copy

2. **UNIVERSITIES AND COLLEGES**

Australian Defence Force Academy
Library
Head of Aerospace and Mechanical Engineering
Deakin University, Serials Section (M list)), Deakin University Library,
Senior Librarian, Hargrave Library, Monash University
Librarian, Flinders University

3. **OTHER ORGANISATIONS**

NASA (Canberra)
AGPS
State Library of South Australia
Parliamentary Library, South Australia

OUTSIDE AUSTRALIA

4. **ABSTRACTING AND INFORMATION ORGANISATIONS**
INSPEC: Acquisitions Section Institution of Electrical Engineers
Library, Chemical Abstracts Reference Service
Engineering Societies Library, US
American Society for Metals
Documents Librarian, The Center for Research Libraries, US

5. **INFORMATION EXCHANGE AGREEMENT PARTNERS**

Acquisitions Unit, Science Reference and Information Service, UK
Library - Exchange Desk, National Institute of Standards and Technology, US

SPARES (10 copies)

Total number of copies: 69

Department of Defence

DOCUMENT CONTROL DATA SHEET

1. Page Classification UNCLASSIFIED	
2. Privacy Marking/Caveat (of document) N/A	

3a. AR Number AR-009-940	3b. Laboratory Number DSTO-RR-0091	3c. Type of Report DSTO RESEARCH REPORT	4. Task Number DST 95/311	
5. Document Date December 1996	6. Cost Code 821931	7. Security Classification	8. No of Pages	32
10. Title Geometric and Radiometric Image Warping due to Displacement of Wide Field Optical Systems		* U (Document) U (Title) U (Abstract) S (Secret) C (Confi) R (Rest) U (Unclas * For UNCLASSIFIED docs with a secondary distribution LIMITATION, use (L) in document box.	9. No of Refs	23
11. Author(s) Robert S. Caprari		12. Downgrading/Delimiting Instructions		
13a. Corporate Author and Address Electronics & Surveillance Research Laboratory PO Box 1500, Salisbury SA 5108		14. Officer/Position responsible for Security:.....CLSOD Downgrading:.....CLSOD Approval for Release: .....CLSOD.		
13b. Task Sponsor DST				

15. Secondary Release Statement of this Document
Approved for public release.

16a. Deliberate Announcement
No limitation.

16b. Casual Announcement (for citation in other documents)
No limitation.

17. DEFTEST Descriptors	18. DISCAT Subject Codes
Geometrical optics; radiometry; wide field optics; precision image registration; approximate image registration; optical system displacement; image warping; geometric warping; radiometric warping; fish-eye lens; imaging characteristic.	

19. Abstract
This report investigates a problem that arises in the precise registration of images viewed from a moving wide field imaging sensor, such as an airborne missile threat warner. It analyses the geometry and radiometry of image formation by idealised, but otherwise arbitrary, imaging optics, thereby determining the image plane irradiance distribution. The analysis extends to determining the transformation of the irradiance (i.e. image warping) due to arbitrary displacement of the optical system; such image warping being separable into geometric (i.e. image point shift) and radiometric (i.e. intensity scaling) components. Numerical simulations demonstrate the severity of the radiometric warping for wide field images-an especially important result, since radiometric warping is conventionally neglected in image registration. Exact solutions for the warping due to pure rotation of an idealised imager are presented. These are completely independent of the scene. An examination of the inclusion of imager translation shows that the warping becomes formally dependent on the scene topography, and emission/scattering directionality. Simulations of the use of block matching to achieve approximate registration are presented.